American Mineralogist, Volume 107, pages 413–420, 2022

Electrical conductivity of metasomatized lithology in subcontinental lithosphere

Ye Peng[1,*], Geeth Manthilake[2], and Mainak Mookherjee[1]

[1]Earth Materials Laboratory, Department of Earth, Ocean and Atmospheric Sciences, Florida State University, Tallahassee, Florida 32306, U.S.A.
[2]Laboratoire Magmas et Volcans, CNRS, IRD, OPGC, Université Clermont Auvergne, Clermont-Ferrand 63000, France

Abstract

A plausible origin of the seismically observed mid-lithospheric discontinuity (MLD) in the subcontinental lithosphere is mantle metasomatism. The metasomatized mantle is likely to stabilize hydrous phases such as amphiboles. The existing electrical conductivity data on amphiboles vary significantly. The electrical conductivity of hornblendite is much higher than that of tremolite. Thus, if hornblendite truly represents the amphibole varieties in MLD regions, then it is likely that amphibole will cause high electrical conductivity anomalies at MLD depths. However, this is inconsistent with the magnetotelluric observations across MLD depths. Hence, to better understand this discrepancy in electrical conductivity data of amphiboles and to evaluate whether MLD could be caused by metasomatism, we determined the electrical conductivity of a natural metasomatized rock sample. The metasomatized rock sample consists of ~87% diopside pyroxene, ~9% sodium-bearing tremolite amphibole, and ~3% albite feldspar. We collected the electrical conductivity data at ~3.0 GPa, i.e., the depth relevant to MLD. We also spanned a temperature range between 400 to 1000 K. We found that the electrical conductivity of this metasomatized rock sample increases with temperature. The temperature dependence of the electrical conductivity exhibits two distinct regimes. At low temperatures <700 K, the electrical conductivity is dominated by the conduction in the solid state. At temperatures >775 K, the conductivity increases, and it is likely to be dominated by the conduction of aqueous fluids due to partial dehydration. The main distinction between the current study and the prior studies on the electrical conductivity of amphiboles or amphibole-bearing rocks is the sodium (Na) content in amphiboles of the assemblage. Moreover, it is likely that the higher Na content in amphiboles leads to higher electrical conductivity. Pargasite and edenite amphiboles are the most common amphibole varieties in the metasomatized mantle, and our study on Na-bearing tremolite is the closest analog of these amphiboles. Comparison of the electrical conductivity results with the magnetotelluric observations constrains the amphibole abundance at MLD depths to <1.5%. Such a low-modal proportion of amphiboles could only reduce the seismic shear wave velocity by 0.4–0.5%, which is significantly lower than the observed velocity reduction of 2–6%. Thus, it might be challenging to explain both seismic and magnetotelluric observations at MLD simultaneously.

Keywords: Mid-lithospheric discontinuity (MLD), electrical conductivity, metasomatized rock, diopside, amphibole

Introduction

Recent high-frequency seismic data have revealed a seismic discontinuity in the subcontinental lithosphere at a depth range of 60–160 km. This is often referred to as the mid-lithospheric discontinuity (MLD) and is characterized by a 2–6% reduction in the seismic shear wave velocity (Rychert and Shearer 2009; Romanowicz 2009; Abt et al. 2010; Fischer et al. 2010). The thickness of the discontinuity typically varies between 10–20 km (Fischer et al. 2010).

Although MLDs are found across all cratons, their origin is poorly understood. A variety of mechanisms have been proposed to explain the observed shear wave velocity anomaly at MLD depths (Selway et al. 2015; Karato et al. 2015). The most plausible mechanisms include: the presence of partial melts (Thybo 2006), elastically accommodated grain boundary sliding (Karato et al. 2015; Karato and Park 2019), seismic anisotropy (Yuan and Romanowicz 2010; Sodoudi et al. 2013; Wirth and Long 2014; Ford et al. 2016), and mantle metasomatism or frozen-in melts (Savage and Silver 2008; Sodoudi et al. 2013; Hansen et al. 2015; Rader et al. 2015; Selway et al. 2015; Saha et al. 2018, 2021; Peng and Mookherjee 2020).

Mantle metasomatism alters the “dry” mantle lithology and often stabilizes carbonates and hydrous minerals such as amphiboles and phlogopite. The xenoliths formed at pressures associated with MLD depths indicate that at least ~25% of them are amphibole-bearing, ~90% are phlogopite-bearing, and less contain carbonates (Rader et al. 2015). While the presence of amphiboles in MLD tends to lower the seismic shear wave velocity (Selway et al. 2015; Peng and Mookherjee 2020; Saha et al. 2021), it may also lead to anomalously high electrical conductivity based on the measurement of hornblendite (Wang et

* E-mail: yp16b@my.fsu.edu. Orcid 0000-0002-9613-7217

0003-004X/22/0003–413$05.00/DOI: https://doi.org/10.2138/am-2021-7942

al. 2012). The study showed that when the temperature is higher than ~760–840 K, the electrical conductivity of hornblendite is enhanced due to the dehydration-oxidation reaction, which is about 10^4–10^6 higher than that of olivine (Wang et al. 2012). This, however, is contrary to magnetotelluric (MT) observations since there is no globally recognized anomaly in the electrical conductivity at MLD depths (Meqbel et al. 2014; Yang et al. 2015; Selway 2019; Karato and Park 2019). The inconsistency between the MT observations and expected electrical conductivity is one of the biggest criticisms of the mantle metasomatism mechanism (Karato and Park 2019). However, a recent experimental study found that the electrical conductivity of tremolite amphibole is much lower than previously thought, about 10^3–10^5 lower than that of hornblendite. It only exceeds the conductivity of olivine by one order of magnitude at temperatures <1123 K, i.e., the melting temperature (Shen et al. 2020). Therefore, the role of amphiboles in the electrical conductivity of the mantle is ambiguous, and it certainly requires further study.

To better understand the effect of hydrous phases on the electrical conductivity of metasomatized lithology, we conducted experiments to constrain the electrical conductivity on a natural metasomatized rock consisting dominantly of pyroxene, amphibole, and feldspar under conditions relevant for MLD, i.e., at ~3.0 GPa and ~400–1000 K. We then used the experimental results to determine the conductivity-depth profiles for the metasomatized cratonic mantle and evaluate whether mantle metasomatism, i.e., metasomatic amphiboles, will cause anomalously high electrical conductivity at MLD depths.

Methods

We characterized the mineral phases of the natural rock sample using Raman spectroscopy at ambient conditions (Fig. 1). To identify the minerals, we used a HORIBA LabRAM HR Evolution Raman spectrometer with a Nd:YAG laser (λ = 532 nm) at the Earth Materials Laboratory, Department of Earth, Ocean, and Atmospheric Sciences, Florida State University, Tallahassee. We also investigated the composition of each mineral phase using electron probe microanalysis (EPMA). We used Cameca SxFive-Tactis at the Laboratoire Magmas et Volcans, Clermont-Ferrand, France, with an accelerating voltage of 15 kV and a steady beam current of 20 nA. We also obtained energy-dispersive X-ray spectroscopy (EDS) chemical mapping of the sample using a JEOL JSM-5910LV scanning electron microscope (SEM) (Online Materials[1] Fig. OM1). We determined the modal abundances using ImageJ open-source package (Schneider et al. 2012). We found that the sample consists of ~87% pyroxene, ~9% amphibole, and ~3% feldspar (Table 1). The stoichiometry of pyroxene is dominated by diopside [$(Mg_{1.02}Ca_{0.85}Na_{0.09}Al_{0.06})(Si_{1.99}Al_{0.01})O_6$], while amphibole is Na-rich tremolite [$(Na_{0.19}K_{0.03})(Ca_{1.61}Na_{0.39})(Mg_{5.09}Fe_{0.02}Ti_{0.01})(Si_{7.75}Al_{0.29})O_{22}(OH)_2$], and feldspar is dominantly albite [$Na_{1.09}K_{0.01}Al_{1.03}Si_{2.94}O_8$] (Table 1).

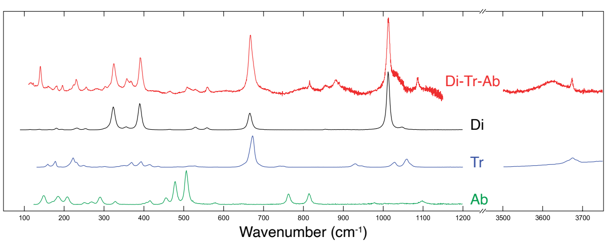

Figure 1. Raman spectrum of the natural metasomatized rock sample containing diopside, tremolite, and albite (Di-Tr-Ab) (red) at ambient conditions. It is compared with the reference Raman spectra for diopside (Di) (RRUFF ID: R040109; black), tremolite (Tr) (RRUFF ID: R040009; blue), and albite (Ab) (RRUFF ID: R040068; green) (Lafuente et al. 2015). (Color online.)

We performed the high-pressure and temperature electrical conductivity experiment in a 1500-ton split-cylinder type multi-anvil apparatus installed at the Laboratoire Magmas et Volcans, Clermont-Ferrand, France. We used an 18/11 assembly, i.e., an edge length of 18 mm for the Cr_2O_3-doped MgO octahedral pressure medium and a truncated edge length of 11 mm for the eight tungsten carbide (WC) anvils. We placed the cylindrical sample specimen in the MgO cylindrical sleeve to electrically insulate the sample from the furnace during the measurements (Online Materials[1] Fig. OM1). In addition, we placed two nickel (Ni) disks at two ends of the sample. These two Ni disks serve as electrodes and also buffer the oxygen fugacity (f_{O_2}) close to Ni-NiO buffer. We monitored the temperature of the sample using a $W_{95}Re_5$-$W_{74}Re_{26}$ thermocouple junction placed at one side of the sample. We placed another $W_{95}Re_5$ wire at the opposite side of the sample and used two opposing $W_{95}Re_5$ wires that emerged at the top and bottom of the sample to collect the impedance spectra for the electrical conductivity measurements. We used a 25 μm thick Re foil as the furnace. To enhance effective heating and minimize thermal loss, i.e., to insulate, we also used a ZrO_2 sleeve surrounding the Re-furnace (Online Materials[1] Fig. OM1). To eliminate the influence of absorbed moisture from the atmosphere and exposure to contaminations, we baked the ceramic assembly parts in a high-temperature furnace at 1273 K for >12 h. We stored all the heat-treated ceramic parts in a high-vacuum furnace (<100 mTorr) at 398 K overnight.

For the electrical conductivity measurements, we analyzed the impedance spectroscopy using the ModuLabMTS impedance/gain-phase analyzer over a frequency range of 10^6–10^1 Hz. Before measuring the temperature dependence of the electrical conductivity of the sample, first, we held the pressure constant at 3.0 GPa and kept the sample at 500 K for more than 6 h. While maintaining a constant temperature of 500 K, we measured the electrical resistance of the sample at regular time intervals to ensure that the sample resistance reached a steady value. We noted that the steady-state resistance is about one order of magnitude lower than the resistance measured at the very beginning (Fig. 2). This step is crucial to ensure the removal of the absorbed moisture in the assembly, which could otherwise influence the electrical conductivity measurements at higher temperatures (Manthilake et al. 2015). Then we collected the impedance spectra over a temperature range of 300–1000 K at a step of ~50 K. Below 700 K, we heated and cooled the sample and found that the electrical resistance for the heating and cooling path was reproducible. This minimizes the uncertainty of the electrical conductivity measurements. After this heating and cooling cycle, we collected the spectra in a continuous heating and cooling cycle reaching 1000 K.

Following the electrical conductivity measurements, we investigated the cross-section of the experimental run product using EPMA and EDS chemical mapping using SEM. We identified the chemical compositions of each mineral phase after the dehydration reaction (Table 1).

The impedance spectra of a polycrystalline sample can be better understood in terms of a resistor-capacitor (R-C) or resistor-constant phase element (R-CPE) circuit. We obtained the resistance of the polycrystalline sample by fitting the impedance spectra to appropriate RC/R-CPE circuits. We determined the electrical conductivity of the sample by the formulation: $\sigma = L/(RS)$, where σ is the electrical conductivity in "S/m," R is the resistance in "Ω", L is the length of the cylindrical sample in "m", and S is the cross-sectional area of the cylindrical sample in "m^2." The sample length and diameter measured before the experiment were ~1.7 and ~1.0 mm, respectively. Similar aspect ratios have been successfully used in previous electrical conductivity measurements, particularly when the samples are cored out of natural rocks rather than synthesized using hot-pressed methods from powdered samples (Manthilake et al. 2015, 2016, 2021). After we recovered the sample, we measured the sample length ~1.7 mm, i.e., it remained unchanged. This is very likely due to the facts that the sample used in our study is a natural rock rather than a powdered sample, and the experimental conditions were modest ~3 GPa, which did not affect the length of the sample. Since the sample was cut and polished along the length of the cylindrical core, we were unable to directly measure the diameter of the recovered sample. Based on the fact that the length remained unaffected, we used the length and diameter of the sample before the experiments to estimate the electrical conductivity.

To ensure that we are measuring the electrical conductivity of the sample and our results are not affected by the sample assembly, we also measured the electrical resistivity of the assembly. The electrical resistivity of the sample is much lower than that of the insulation resistance of the sample assembly (MgO), i.e., the electrical conductivity of the sample is significantly greater than that of the assembly (Online Materials[1] Fig. OM2).

Results

We analyzed the electrical conductivity of the sample using the impedance spectra, which are often represented in a Cole-Cole plot with the imaginary part of the impedance plotted

Table 1. Chemical composition (wt%) of mineral phases in the sample assemblage determined by EPMA before and after the electrical conductivity measurements

Sample	SiO_2	MgO	CaO	Al_2O_3	Na_2O	K_2O	FeO	TiO_2	Cr_2O_3	NiO	MnO	Total	Modal abundance
Before													
Di	$(Mg_{1.02}Ca_{0.85}Na_{0.09}Al_{0.06})(Si_{1.99}Al_{0.01})O_6$												87.5%
	55.58	19.10	22.03	1.62	1.25	0.00	0.12	0.02	0.04	0.09	–	99.86	
Tr	$(Na_{0.19}K_{0.03})(Ca_{1.61}Na_{0.39})(Mg_{5.09}Fe_{0.02}Ti_{0.01})(Si_{7.75}Al_{0.29})O_{22}(OH)_2$												9.1%
	58.27	25.68	11.28	1.83	2.24	0.17	0.17	0.14	0.04	0.04	–	99.87	
Ab	$(Na_{1.09}K_{0.01})Al_{1.03}Si_{2.94}O_8$												3.4%
	66.70	0.37	0.07	19.77	12.79	0.11	0.04	0.03	0.02	0.09	–	99.97	
After													
Di	$(Ca_{0.96}Na_{0.04})(Mg_{0.95}Al_{0.04})Si_{2.00}O_6$												87.2%
	55.94	17.76	24.95	0.87	0.54	0.00	0.18	0.03	0.04	–	0.17	100.49	
Tr	$(Na_{0.38}K_{0.05})(Ca_{1.73}Na_{0.27})(Mg_{4.69}Al_{0.17}Ti_{0.06}Fe_{0.03}Mn_{0.02})(Si_{7.61}Al_{0.39})O_{22}(OH)_2$												9.1%
	57.15	23.24	12.29	2.50	1.69	0.19	0.26	0.34	0.03	–	0.18	97.89	
Ab	$(Na_{0.96}K_{0.01}Mg_{0.01}Ca_{0.01})Al_{1.01}Si_{2.99}O_8$												3.4%
	69.32	0.03	0.32	19.88	11.41	0.16	0.01	0.00	0.00	–	0.01	101.15	
Loss													0.3%

Notes: The chemical composition of each phase is slightly modified after the experiment. Di = diopside, Tr = tremolite, Ab = albite.

in the ordinate, and the real part of the impedance plotted in the abscissa. At low temperatures, <700 K, all the spectra display a semicircular arc over the whole frequency range (Online Materials[1] Fig. OM3). The radius of the semicircular arc is proportional to the electrical resistivity, i.e., inversely proportional to the electrical conductivity. With increasing temperature, the radius of the semicircular arc continues to shrink, indicating that the electrical resistivity reduces or conversely the electrical conductivity increases with temperature. At temperatures >775 K, an additional arc is observed in the low-frequency range (Online Materials[1] Fig. OM3). The separation of the two arcs possibly indicates two conductive paths: one through the grain interior and the other along the grain boundary. This is very likely due to the dehydration of the amphibole-bearing rock sample, which generates two conductive phases operating in series, i.e., the original solid phase and the aqueous fluid phase interconnected along the grain boundaries.

The temperature dependence of the electrical conductivity exhibits a linear relationship before and after dehydration, and both could be well described by the Arrhenius relationship:

$$\sigma = \sigma_0 \exp\left(\frac{-\Delta H}{RT}\right) \tag{1}$$

where σ_0 is a pre-exponential constant, R is the gas constant, and ΔH is the activation enthalpy. The activation enthalpies are, respectively, 0.188 ± 0.003 eV and 0.48 ± 0.03 eV before and after dehydration (Fig. 2; Table 2). The increase in the activation enthalpy of the different segments is likely due to the dehydration

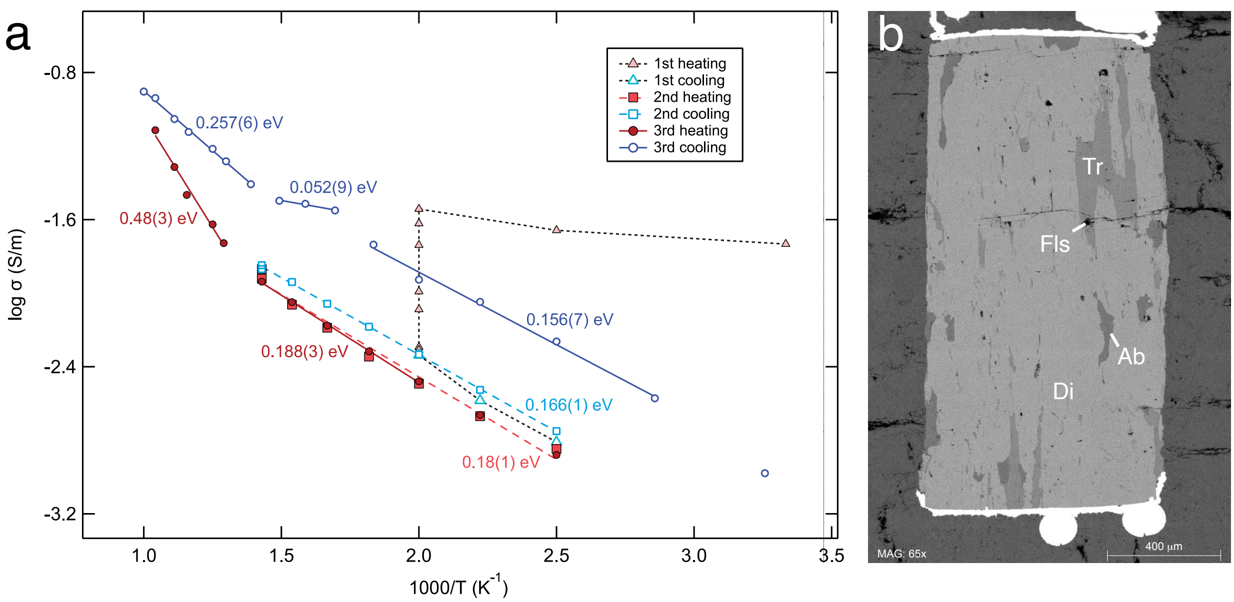

Figure 2. (**a**) Electrical conductivity of diopside-tremolite-albite sample as a function of reciprocal temperature. The sample was subjected to several heating-cooling cycles. The lines represent Arrhenius fits to the data, except for the first heating-cooling cycle. The colored numbers indicate the activation enthalpy associated with each regime, i.e., solid-state conduction and partial dehydration. (**b**) SEM image of the sample after the electrical conductivity experiment. The mineral phases are labeled. Locally interconnected thin bands of tremolite phase are noted. Abbreviation: Di = diopside, Tr = tremolite, Ab = albite, Fls = fluids. (Color online.)

reaction of the amphibole phase in the sample. The release of aqueous fluids often causes the change of slope, i.e., activation enthalpy in the temperature-dependent electrical conductivity of hydrous phases. The activation enthalpy after dehydration obtained in our study, i.e., the T_2 segment between 775 and 1000 K, is very similar to the activation enthalpy ~0.5 eV in the T_3 segment of the tremolite sample, where the conduction mechanism is dominant by the flow of aqueous fluids (Shen et al. 2020) (Fig. 3; Table 2).

The temperature range where the slope change occurs generally depends on the specific mineral assemblage and its thermal stability (Manthilake et al. 2015, 2016; Pommier and Evans 2017; Pommier et al. 2019). The experimental study on pargasitic-edenitic amphiboles indicates that these amphibole phases are stable till 1373 K (Mandler and Grove 2016). However, in our study, amphibole starts to dehydrate at ~775 K. An earlier study on the hornblende-actinolite-bearing rock (hornblendite) at 0.5 GPa exhibits two distinct stages of the temperature dependence of electrical conductivity, and the slope changes at ~736–760 K. Similarly, the plagioclase-hornblende-bearing rock (plagioclase hornblendite) also undergoes the discontinuous increase of the electrical conductivity at similar temperatures, i.e., ~797–840 K (Fig. 3; Table 2) (Wang et al. 2012). It is not surprising that amphiboles show much lower dehydration temperatures in a multi-phase rock. The stability field of amphiboles decreases when competing with other phases, like diopside and albite.

We also noted that the electrical conductivity of our diopside-tremolite-albite sample is higher than that of pure clinopyroxene (Yang et al. 2011) or pure tremolite (Shen et al. 2020) by a factor of 10^3–10^4, especially when the temperature is lower than 1000 K (Fig. 3). These electrical conductivity experiments on clinopyroxene, plagioclase, and amphibole were conducted at different pressures. The effect of pressure on the electrical conductivity is found to be negligible (Yang et al. 2011, 2012; Shen et al. 2020; Hu et al. 2018). Recent experiments on Fe-bearing amphibole indicated that the total Fe content influences the electrical conductivity of amphiboles. Upon heating, the sample loses hydrogen and in the process oxides the iron ($Fe^{2+} \rightarrow Fe^{3+}$), which in turn enhances the electrical conductivity via hopping of electrons (Hu et al. 2018). However, the total Fe content of our sample is as low as ~0.12 wt%, and yet we found that our electrical conductivity results are very high, especially in the solid state (Fig. 3). This high electrical conductivity cannot be attributed to Fe content. We found that the Na_2O content in our sample, 2.24 wt%, is greater than that of all the amphibole samples examined in earlier

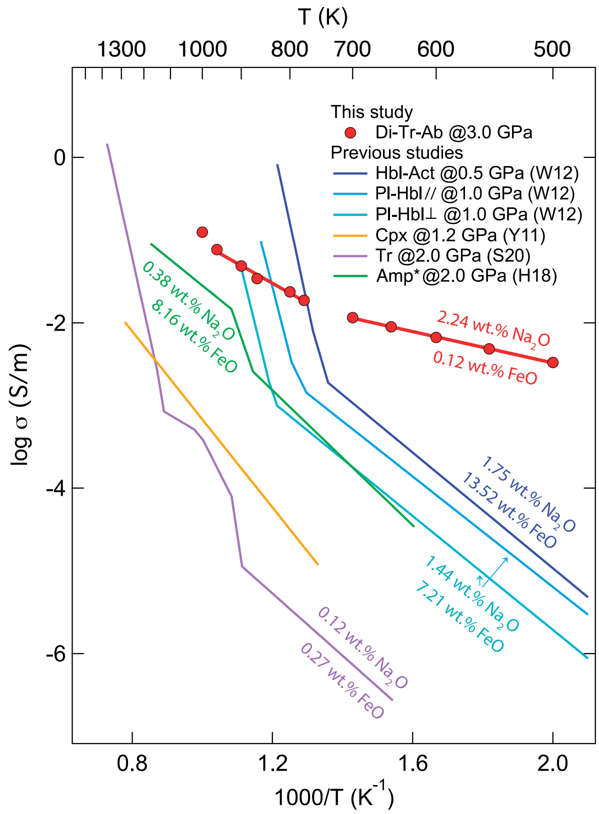

FIGURE 3. Plot of electrical conductivity of the diopside-tremolite-albite (Di-Tr-Ab) sample as a function of reciprocal temperature. The colored numbers indicate the Na_2O content in the amphibole phase of the samples and the total FeO content of the samples. Note: filled red symbols = data from this study; bold red lines = Arrhenius fit to data from this study; dark blue line = hornblende-actinolite-bearing hornblendite (Hbl-Act) (W12 = Wang et al. 2012); intermediate blue line = plagioclase-hornblende-bearing hornblendite parallel to the lineation within the sample (Pl-Hbl//); light blue line = plagioclase-hornblende-bearing hornblendite perpendicular to the lineation within the sample (Pl-Hbl^); orange line = clinopyroxene (Cpx) (Y11 = Yang et al. 2011); purple line = tremolite (Tr) (S20 = Shen et al. 2020); and the green line = amphibole (Amp) (H18 = Hu et al. 2018). * We note an unreasonable high CaO content ~20.43 wt% in the amphibole sample (Hu et al. 2018). This might indicate that the amphibole sample is not representative of the lithosphere. The relevant CaO content for amphiboles that are likely to be stable in the metasomatized mantle ranges between 9.2–12.6 wt% (Saha et al. 2021). (Color online.)

TABLE 2. Arrhenius fit parameters of the diopside-tremolite sample in this study and previous studies with experimental pressure and temperature conditions

Mineral phase	P (GPa)	T_1 (K)	$\log\sigma_{01}$ (S/m)	ΔH_1 (eV)	T_2 (K)	$\log\sigma_{02}$ (S/m)	ΔH_2 (eV)	T_3 (K)	$\log\sigma_{03}$ (S/m)	ΔH_3 (eV)	T_4 (K)	$\log\sigma_{04}$ (S/m)	ΔH_4 (eV)	Reference
Di-Tr-Ab	3.0	450–700	−0.59(3)	0.188(3)	775–1000	1.4(2)	0.48(3)	–	–	–	–	–	–	This study
Hbl-Act	0.5	420–736	2.03(9)	0.69(2)	760–824	24(2)	3.9(4)	–	–	–	–	–	–	Wang et al. (2012)
Pl+Hbl(^)	1.0	443–824	1.18(7)	0.68(1)	840–900	18.0(7)	3.5(2)	–	–	–	–	–	–	Wang et al. (2012)
Pl+Hbl(//)	1.0	395–771	1.49(7)	0.66(1)	797–857	18(2)	3.3(4)	–	–	–	–	–	–	Wang et al. (2012)
Tr	2.0	648–898	−0.8(2)	0.75(3)	923–998	5.0(9)	1.7(2)	1023–1123	−1(1)	0.5(2)	1148–1373	14.2(6)	3.8(2)	Shen et al. (2020)
Cpx	1.2	773–1273	2.2(3)	1.06(5)	–	–	–	–	–	–	–	–	–	Yang et al. (2011)
Pl	1.2	773–1273	4.1(3)	1.67(6)	–	–	–	–	–	–	–	–	–	Yang et al. (2012)
Amp[a]	2.0	623–873	2.08	0.81	923–1173	1.88	0.68	–	–	–	–	–	–	Hu et al. (2018)

Notes: The numbers in parentheses are the error of the last digit with one standard deviation. Di = diopside, Tr = tremolite, Ab = albite, Hbl = hornblende, Act = actinolite, Pl = plagioclase, Cpx = clinopyroxene, Amp = amphibole.

[a] We note an unreasonable high CaO content ~20.43 wt% in the amphibole sample (Hu et al. 2018). This might indicate that the amphibole sample is not representative of the lithosphere. The relevant CaO content for amphiboles that are likely to be stable in the metasomatized mantle ranges between 9.2–12.6 wt% (Saha et al. 2021).

electrical conductivity studies, i.e., 0.12 wt% in tremolite (Shen et al. 2020); ~0.38 wt% in Fe-bearing amphibole (Hu et al. 2018) and 1.44–1.75 wt% in amphibole-bearing rocks (Wang et al. 2012). The alkali cation, i.e., Na, occupies the alkali (A) site in the crystal structure of amphiboles and the A site is often vacant in many amphibole end-members, including tremolite. It is very likely that Na is loosely bound in the large A site in amphiboles. The A sites are connected to each other to form channels along [001] direction that is likely to further facilitate the mobility of the Na^+ ions. Similar high electrical conductivity has been observed in liebermannite, which also has tunnels that promote the migration of alkali cations (He et al. 2016; Manthilake et al. 2020). Also, fast ionic conduction in the solid state has been observed in albite, where Na^+ ions undergo faster diffusion via the alkali ion cavities in the albite aluminosilicate framework (Hu et al. 2011). Thus, it is very likely that Na content significantly affects the electrical conductivity of amphiboles (Fig. 3). When we compare our electrical conductivity data with prior results on amphibole-bearing samples, we found a strong correlation between the electrical conductivity and the Na_2O content, i.e., as the Na_2O content in the amphibole phase of the sample increases, the electrical conductivity is enhanced (Fig. 3). The activation enthalpy for our sample at lower temperatures, i.e., in the solid state, is also much lower than that of the samples with lower Na content (Fig. 3; Table 2).

The electrical conductivity of major mantle mineral phases [nominally anhydrous mineral (NAM) phases], including olivine (Gardés et al. 2014; Xu et al. 2000; Wang et al. 2006; Yoshino et al. 2006, 2009; Dai et al. 2010; Dai and Karato 2014a, 2014b; Fei et al. 2020), pyroxene (Dai and Karato 2009a), and garnet (Dai and Karato 2009b) is lower than that of amphiboles or amphibole-bearing rocks (Online Materials[1] Fig. OM4). One exception is that the electrical conductivity of orthopyroxene is slightly higher than that of pure tremolite (Yang et al. 2012; Shen et al. 2020). However, trace amounts of water/hydrogen often have a significant impact on the electrical conductivity because hydrogen atoms in NAMs occur as defects and are not structurally bonded (Karato 1990; Wang et al. 2006). For example, the electrical conductivity of garnet with ~50 ppm of water is quite comparable to those of Na-rich amphiboles or amphibole-bearing rocks at mid-lithosphere temperatures. While the electrical conductivity of volumetrically dominant mantle phases at MLD conditions, i.e., olivine and pyroxene with ~50 ppm of water, is still lower than those of Na-rich amphiboles but comparable with Na-poor amphiboles (Online Materials[1] Fig. OM4).

Discussion

To test whether mantle metasomatism could be a plausible cause for MLD, we selected a natural metasomatized rock sample that consists of ~87% diopside, ~9% tremolite, and ~3% albite. The electrical conductivity of the diopside is similar to that of orthopyroxene (Yang et al. 2011, 2012) and slightly higher than that of olivine (Gardés et al. 2014). The metasomatized cratonic mantle often contains <10% amphiboles. To recreate chemistry and modal abundances of mineral phases in the metasomatized mantle, recent experimental studies have demonstrated that 90 wt% depleted mantle rock and 10 wt% rhyolitic melts could generate 3.6 to 9.4% amphiboles over 2–3 GPa and 1223–1323 K (Saha et al. 2018). Thus, our selected metasomatized sample with ~9% amphibole is a good representative for the metasomatized cratonic mantle rock.

Owing to the low-modal abundance of amphiboles in the metasomatized mantle, it is very unlikely that they are interconnected. However, amphibole-bearing xenoliths do suggest that amphiboles might be connected via veins (Ionov and Hofmann 1995). In our experiment, the texture of the starting sample does not show any evidence for the interconnectivity of the amphibole (Online Materials[1] Fig. OM1). However, the SEM image of the sample after the electrical conductivity measurement shows that tremolite develops a texture that resembles discontinuous and locally interconnected thin veins that are near perpendicular to the electrodes (Fig. 2). These thin veins are not inherent to the sample and very likely represent quenched aqueous fluids along the grain boundaries.

In the earlier electrical conductivity study on tremolite, the sample had little Na. In contrast, our sample assemblage contains Na-bearing tremolite and albite, and is more representative of the metasomatized mantle rock in MLD. It is well known that tremolite and albite may form edenite amphiboles at higher pressures (Spear 1981). Tremolite + tschermakite amphibole + albite could form pargasite amphibole at higher pressures (Bhadra and Bhattacharya 2007). It is also well known that the most relevant phase of amphiboles stable at MLD conditions is pargasitic-edenitic amphiboles (Mandler and Grove 2016; Saha et al. 2018), which translates to 3.4–4.4 wt% Na_2O content in amphiboles (Saha et al. 2018). The even higher Na content in MLD indicates that the electrical conductivity is likely to be similar or higher than our electrical conductivity results. Such a high conductivity is very likely to cause a positive anomaly. This is, however, not detected by MT observations and thus puts severe constraints on metasomatism as a viable mechanism to explain MLD.

Implications

Our experimental electrical conductivity data can provide independent and important constraints on the debated mechanism of MLD, i.e., mantle metasomatism. To better evaluate the electrical conductivity of the metasomatized mantle, we used our results on the temperature dependence of the electrical conductivity of diopside-tremolite-albite rock and extrapolated to conditions relevant for MLD. We calculated the electrical conductivity vs. depth along a typical steady-state conductive geotherm of the cratonic lithosphere, with a surface heat flux of 45 mW/m^2 (Lee et al. 2011) (Fig. 4). We extrapolated the electrical conductivity of the solid-state regime to MLD depths. To compare with pristine mantle free from any metasomatism, we determined electrical conductivity-depth profiles using a depleted peridotite composition consisting of ~48.5% olivine, ~41.5% orthopyroxene, ~9.1% garnet, and ~0.9% clinopyroxene. This mantle rock model is based on the average composition of the global cratonic xenoliths (Saha et al. 2018; Lee et al. 2011; Luguet et al. 2015; Maier et al. 2012; Pearson and Wittig 2013). We also considered the effect of enhanced electrical conductivity due to hydrogen defects in NAMs. As is well-known, cratons are stable, which indicates cratons are rheologically stiff and often dry so that they resist being swept away by mantle convection.

However, recent studies have shown that most of the cratonic lithospheric mantle is not as dry as assumed and can contain a small amount of water in NAMs such that it will not affect the overall rheological strength of the craton, i.e., it can sustain over geological times (Selway 2019; Demouchy and Bolfan-Casanova 2016; Griffin et al. 2009; Saal et al. 2002; Simons et al. 2002; Freitas and Manthilake 2019). Thus, we considered two distinct cases for the unmetasomatized "background" mantle: (1) major mantle minerals are "dry," and (2) major mantle minerals are "wet" with an aggregate water content of 50 ppm (Saal et al. 2002; Simons et al. 2002; Freitas and Manthilake 2019). We also considered the partition coefficients of water among these major mantle phases from earlier studies for the "wet" model (Ardia et al. 2012; Férot and Bolfan-Casanova 2012; Demouchy and Bolfan-Casanova 2016; Mookherjee and Karato 2010).

To estimate the electrical conductivity of the unmetasomatized "background" mantle, we used the generalized Archie's Law (Glover 2010):

$$\sigma = \sum_{i}^{n} \sigma_i \phi_i^{m_i} \tag{2}$$

where σ_i is the electrical conductivity of the i^{th} mineral phase ($i = 1,2,...,n$), ϕ_i is the modal abundance of the i^{th} mineral phase, and m_i is the connectivity exponent of the i^{th} mineral phase, which is inversely related to the physical connectivity of mineral phase. We used the connectivity exponent $m_i = 1.3$ for the i^{th} phase comprising ≥20% of the whole rock, $m_i = 2$ for the phase comprising 10–20%, and $m_i = 3$ for the phase comprising <10% (Selway 2019). For an ideal connection, $m = 1$.

We calculated the electrical conductivity of two distinct lithologies by combining the electrical conductivity of metasomatized rock, i.e., our study, with (1) "dry background" mantle and (2) "wet background" mantle. We compared the predicted electrical conductivity-depth profiles with available MT data (Yang et al. 2015) near two distinct seismic stations JFWS and EYMN located in the northern U.S. (Selway 2019). These two stations have reported MLDs at depths of 59 and 94 km, respectively (Abt et al. 2010). To explain the MT observations, we varied the proportion of the depleted peridotite rock and the metasomatized rock.

We found that at the MLD depth, i.e., ~60–95 km in the northern U.S., the conductivity of our metasomatized rock is 3.1–4.6 orders of magnitude greater than the "dry" depleted mantle and 1.6–2.4 orders of magnitude greater than the "wet" depleted mantle with 50 ppm of water (Fig. 4). The difference between the electrical conductivity of the "dry" and "wet" depleted mantle is due to the effect of extrinsic hydrogen defects. We also found that if the sub-cratonic mantle is "dry," the lower bound of the observed MT profile could be explained by ~7% of partial metasomatism. This means ~0.6% amphiboles in the bulk rock. Meanwhile the upper bound could be explained by partial metasomatism not exceeding 17%, which is equivalent to ~1.5% amphibole in the bulk rock. In the "wet" mantle, we noted that without the effect of mantle metasomatism, it is already sufficient to explain the observed MT profiles. And the upper bound of the MT profiles could be explained by <14% of partial metasomatism, i.e., <1.3% amphibole in the bulk rock (Fig. 4). However, ~1.5% amphibole in the bulk rock could only reduce the seismic shear wave velocity by ~0.4–0.5% at MLD depths (Saha et al. 2021; Peng and Mookherjee 2020), while a 2–6% reduction in the seismic shear wave velocity has been observed in most MLD regions (Rychert and Shearer 2009; Romanowicz

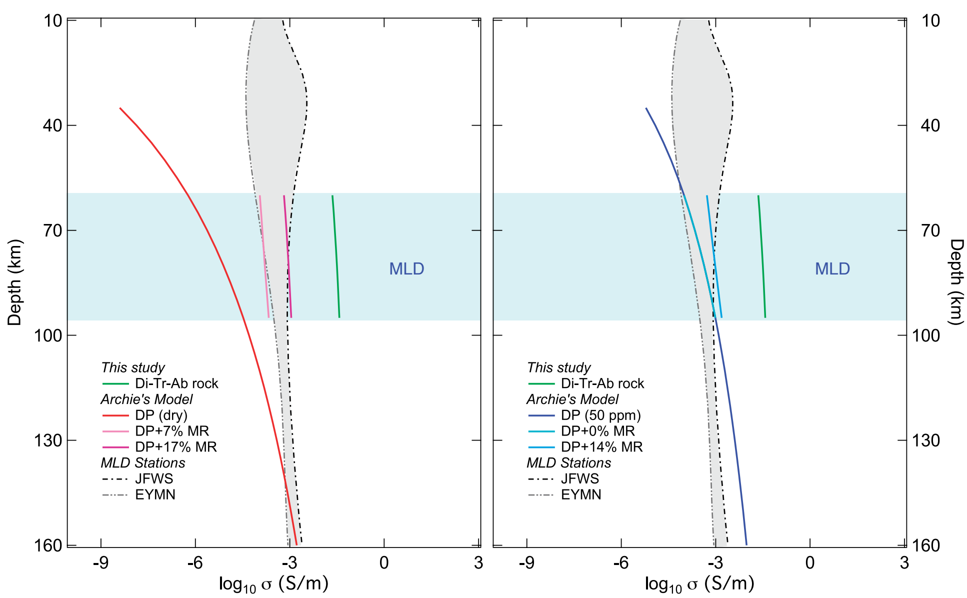

FIGURE 4. The conductivity-depth profile of the diopside-tremolite-albite sample (Di-Tr-Ab) (green lines) and predicted conductivity-depth profiles of the (**a**) "dry" and (**b**) "wet" (50 ppm of water) depleted peridotite (DP) based on the generalized Archie's Law. The lighter red and blue lines are the bulk conductivity of the mixed model. For example, DP + 7% MR means the bulk rock consists of 93% depleted peridotite (DP) and 7% of our metasomatized rock (MR), i.e., the diopside-tremolite-albite sample. The dashed lines indicate the conductivity-depth profiles from the three-dimensional MT models near seismic stations JFWS and EYMN in the northern U.S. (Yang et al. 2015). The cyan shaded area shows the depth range of MLDs reported at the two seismic stations (Abt et al. 2010). (Color online.)

2009; Abt et al. 2010; Fischer et al. 2010). Hence, our results do indicate that irrespective of whether the sub-cratonic mantle is "dry" or "wet," the presence of Na-rich amphibole-bearing rock or mantle metasomatism cannot explain the seismic shear wave velocity and electrical conductivity of MLD simultaneously.

Acknowledgments

The authors thank Zhicheng Jing and the two reviewers Lidong Dai and Hongzhan Fei for their constructive criticism that enhanced the clarity of the article.

Funding

Y.P. and M.M. acknowledge NSF funding EAR 1638752, 1763215, and 1753125. G.M. acknowledges funding from the INSU-CNRS. This research was also financed by the French Government Laboratory of Excellence initiative no. ANR-10-LABX-0006, the Région Auvergne, and the European Regional Development Fund (ClerVolc contribution number 472).

References cited

Abt, D.L., Fischer, K.M., French, S.W., Ford, H.A., Yuan, H., and Romanowicz, B. (2010) North American lithospheric discontinuity structure imaged by P_S and S_P receiver functions. Journal of Geophysical Research, 115, B09301.

Ardia, P., Hirschmann, M.M., Withers, A.C., and Tenner, T.J. (2012) H_2O storage capacity of olivine at 5–8 GPa and consequences for dehydration partial melting of the upper mantle. Earth and Planetary Science Letters, 345-348, 104–116.

Bhadra, S., and Bhattacharya, A. (2007) The barometer tremolite + tschermackite + 2 albite = 2 pargasite + 8 quartz: Constraints from experimental data at unit silica activity, with application to garnet-free natural assemblages. American Mineralogist, 92, 491–502.

Dai, L., and Karato, S.-I. (2009a) Electrical conductivity of orthopyroxene: Implications for the water content of the asthenosphere. Proceedings of the Japan Academy. Series B, Physical and Biological Sciences, 85, 466–475.

——— (2009b) Electrical conductivity of pyrope-rich garnet at high temperature and high pressure. Physics of the Earth and Planetary Interiors, 176, 83–88.

——— (2014a) The effect of pressure on the electrical conductivity of olivine under the hydrogen-rich conditions. Physics of the Earth and Planetary Interiors, 232, 51–56.

——— (2014b) Influence of oxygen fugacity on the electrical conductivity of hydrous olivine: Implications for the mechanism of conduction. Physics of the Earth and Planetary Interiors, 232, 57–60.

Dai, L., Li, H., Li, C., Hu, H., and Shan, S. (2010) The electrical conductivity of dry polycrystalline olivine compacts at high temperatures and pressures. Mineralogical Magazine, 74, 849–857.

Demouchy, S., and Bolfan-Casanova, N. (2016) Distribution and transport of hydrogen in the lithospheric mantle: A review. Lithos, 240-243, 402–425.

Fei, H., Druzhbin, D., and Katsura, T. (2020) The effect of water on ionic conductivity in olivine. Journal of Geophysical Research: Solid Earth, 125, e2019JB019313.

Férot, A., and Bolfan-Casanova, N. (2012) Water storage capacity in olivine and pyroxene to 14 GPa: Implications for the water content of the Earth's upper mantle and nature of seismic discontinuities. Earth and Planetary Science Letters, 349-350, 218–230.

Fischer, K.M., Ford, H.A., Abt, D.L., and Rychert, C.A. (2010) The lithosphere-asthenosphere boundary. Annual Review of Earth and Planetary Sciences, 38, 551–575.

Ford, H.A., Long, M.D., and Wirth, E.A. (2016) Midlithospheric discontinuities and complex anisotropic layering in the mantle lithosphere beneath the Wyoming and Superior Provinces. Journal of Geophysical Research: Solid Earth, 121, 6675–6697.

Freitas, D., and Manthilake, G. (2019) Electrical conductivity of hydrous silicate melts: Implications for the bottom-up hydration of Earth's upper mantle. Earth and Planetary Science Letters, 523, 115712.

Gardés, E., Gaillard, F., and Tarits, P. (2014) Toward a unified hydrous olivine electrical conductivity law. Geochemistry, Geophysics, Geosystems, 15, 4984–5000.

Glover, P.W.J. (2010) A generalized Archie's law for n phases. Geophysics, 75, E247–E265.

Griffin, W.L., O'Reilly, S.Y., Afonso, J.C., and Begg, G.C. (2009) The composition and evolution of lithospheric mantle: A re-evaluation and its tectonic implications. Journal of Petrology, 50, 1185–1204.

Hansen, S.M., Dueker, K., and Schmandt, B. (2015) Thermal classification of lithospheric discontinuities beneath USArray. Earth and Planetary Science Letters, 431, 36–47.

He, Y., Sun, Y., Lu, X., Gao, J., Li, H., and Li, H. (2016) First-principles prediction of fast migration channels of potassium ions in $KAlSi_3O_8$ hollandite: Implications for high conductivity anomalies in subduction zones. Geophysical Research Letters, 43, 6228–6233.

Hu, H., Li, H., Dai, L., Shan, S., and Zhu, C. (2011) Electrical conductivity of albite at high temperatures and high pressures. American Mineralogist, 96, 1821–1827.

Hu, H., Dai, L., Li, H., Sun, W., and Li, B. (2018) Effect of dehydrogenation on the electrical conductivity of Fe-bearing amphibole: Implications for high conductivity anomalies in subduction zones and continental crust. Earth and Planetary Science Letters, 498, 27–37.

Ionov, D.A., and Hofmann, A.W. (1995) Nb-Ta-rich mantle amphiboles and micas: Implications for subduction-related metasomatic trace element fractionations. Earth and Planetary Science Letters, 131, 341–356.

Karato, S.-I. (1990) The role of hydrogen in the electrical conductivity of the upper mantle. Nature, 347, 272–273.

Karato, S.-I., and Park, J. (2019) On the origin of the upper mantle seismic discontinuities. In H. Yuan and B. Romanowicz, Eds., Lithospheric Discontinuities, Geophysical Monograph Series, 239, 5–34. American Geophysical Union. https://doi.org/10.1002/9781119249740.ch1.

Karato, S.-I., Olugboji, T., and Park, J. (2015) Mechanisms and geologic significance of the mid-lithosphere discontinuity in the continents. Nature Geoscience, 8, 509–514.

Lafuente, B., Downs, R.T., Yang, H., and Stone, N. (2015) The power of databases: the RRUFF project. In T. Armbruster and R.M. Danisi, Eds., Highlights in mineralogical crystallography, 1–30. de Gruyter. https://doi.org/10.1515/9783110417104-003.

Lee, C.-T.A., Luffi, P., and Chin, E.J. (2011) Building and destroying continental mantle. Annual Review of Earth and Planetary Sciences, 39, 59–90.

Luguet, A., Behrens, M., Pearson, D.G., König, S., and Herwartz, D. (2015) Significance of the whole rock Re-Os ages in cryptically and modally metasomatised cratonic peridotites: Constraints from HSE-Se-Te systematics. Geochimica et Cosmochimica Acta, 164, 441–463.

Maier, W.D., Peltonen, P., McDonald, I., Barnes, S.J., Barnes, S.J., Hatton, C., and Viljoen, F. (2012) The concentration of platinum-group elements and gold in southern African and Karelian kimberlite-hosted mantle xenoliths: implications for the noble metal content of the Earth's mantle. Chemical Geology, 302-303, 119–135.

Mandler, B.E., and Grove, T.L. (2016) Controls on the stability and composition of amphibole in the Earth's mantle. Contributions to Mineralogy and Petrology, 171, 68.

Manthilake, G., Mookherjee, M., Bolfan-Casanova, N., and Andrault, D. (2015) Electrical conductivity of lawsonite and dehydrating fluids at high pressures and temperatures. Geophysical Research Letters, 42, 7398–7405.

Manthilake, G., Bolfan-Casanova, N., Novella, D., Mookherjee, M., and Andrault, D. (2016) Dehydration of chlorite explains anomalously high electrical conductivity in the mantle wedges. Science Advances, 2, e1501631.

Manthilake, G., Schiavi, F., Zhao, C., Mookherjee, M., Bouhifd, M.A., and Jouffret, L. (2020) The electrical conductivity of liebermannite: Implications for water transport into the Earth's lower mantle. Journal of Geophysical Research: Solid Earth, 125, e2020JB020094.

Manthilake, G., Mookherjee, M., and Miyajima, N. (2021) Insights on the deep carbon cycle from the electrical conductivity of carbon-bearing aqueous fluids. Scientific Reports, 11.

Meqbel, N.M., Egbert, G.D., Wannamaker, P.E., Kelbert, A., and Schultz, A. (2014) Deep electrical resistivity structure of the northwestern U.S. derived from 3-D inversion of USArray magnetotelluric data. Earth and Planetary Science Letters, 402, 290–304.

Mookherjee, M., and Karato, S.-I. (2010) Solubility of water in pyrope-rich garnet at high pressures and temperature. Geophysical Research Letters, 37.

Pearson, D.G., and Wittig, N. (2013) The formation and evolution of cratonic mantle lithosphere – Evidence from mantle xenoliths. In H.D. Holland and K.K. Turekian, Eds., Treatise on Geochemistry, 3, 225–292. Elsevier.

Peng, Y., and Mookherjee, M. (2020) Thermoelasticity of tremolite amphibole: Geophysical implications. American Mineralogist, 105, 904–916.

Pommier, A., and Evans, R.L. (2017) Constraints on fluids in subduction zones from electromagnetic data. Geosphere, 13, GES01473.1–1041.

Pommier, A., Williams, Q., Evans, R.L., Pal, I., and Zhang, Z. (2019) Electrical Investigation of Natural Lawsonite and Application to Subduction Contexts. Journal of Geophysical Research: Solid Earth, 124, 1430–1442.

Rader, E., Emry, E., Schmerr, N., Frost, D., Cheng, C., Menard, J., Yu, C., and Geist, D. (2015) Characterization and petrological constraints of the midlithospheric discontinuity. Geochemistry, Geophysics, Geosystems, 16, 3484–3504.

Romanowicz, B. (2009) The thickness of tectonic plates. Science, 324, 474–476.

Rychert, C.A., and Shearer, P.M. (2009) A global view of the lithosphere-asthenosphere boundary. Science, 324, 495–498.

Saal, A.E., Hauri, E.H., Langmuir, C.H., and Perfit, M.R. (2002) Vapour undersaturation in primitive mid-ocean-ridge basalt and the volatile content of Earth's upper mantle. Nature, 419, 451–455.

Saha, S., Dasgupta, R., and Tsuno, K. (2018) High pressure phase relations of a depleted peridotite fluxed by CO_2-H_2O-bearing siliceous melts and the origin of mid-lithospheric discontinuity. Geochemistry, Geophysics, Geosystems,

19, 595–620.
Saha, S., Peng, Y., Dasgupta, R., Mookherjee, M., and Fischer, K.M. (2021) Assessing the presence of volatile-bearing mineral phases in the cratonic mantle as a possible cause of mid-lithospheric discontinuities. Earth and Planetary Science Letters, 553, 116602.
Savage, B., and Silver, P.G. (2008) Evidence for a compositional boundary within the lithospheric mantle beneath the Kalahari craton from S receiver functions. Earth and Planetary Science Letters, 272, 600–609.
Schneider, C.A., Rasband, W.S., and Eliceiri, K.W. (2012) NIH Image to ImageJ: 25 years of image analysis. Nature Methods, 9, 671–675.
Selway, K. (2019) Electrical discontinuities in the continental lithosphere imaged with magnetotellurics. In H. Yuan and B. Romanowicz, Eds., Lithospheric Discontinuities, Geophysical Monograph Series, 239, p. 89–109. American Geophysical Union. https://doi.org/10.1002/9781119249740.ch5.
Selway, K., Ford, H., and Kelemen, P. (2015) The seismic mid lithosphere discontinuity. Earth and Planetary Science Letters, 414, 45–57.
Shen, K., Wang, D., and Liu, T. (2020) Electrical conductivity of tremolite under high temperature and pressure: implications for the high-conductivity anomalies in the Earth and Venus. Contributions to Mineralogy and Petrology, 175, 52.
Simons, K., Dixon, J., Schilling, J.G., Kingsley, R., and Poreda, R. (2002) Volatiles in basaltic glasses from the Easter-Salas y Gomez Seamount Chain and Easter Microplate: Implications for geochemical cycling of volatile elements. Geochemistry, Geophysics, Geosystems, 3, 1–29.
Sodoudi, F., Yuan, X., Kind, R., Lebedev, S., Adam, J.M.C., Kästle, E., and Tilmann, F. (2013) Seismic evidence for stratification in composition and anisotropic fabric within the thick lithosphere of Kalahari Craton. Geochemistry, Geophysics, Geosystems, 14, 5393–5412.
Spear, F.S. (1981) Amphibole-plagioclase equilibria: an empirical model for the relation albite + tremolite = edenite + 4 quartz. Contributions to Mineralogy and Petrology, 77, 355–364.
Thybo, H. (2006) The heterogeneous upper mantle low velocity zone. Tectonophysics, 416, 53–79.
Wang, D., Mookherjee, M., Xu, Y., and Karato, S.-I. (2006) The effect of water on the electrical conductivity of olivine. Nature, 443, 977–980.
Wang, D., Guo, Y., Yu, Y., and Karato, S.-I. (2012) Electrical conductivity of amphibole-bearing rocks: Influence of dehydration. Contributions to Mineralogy and Petrology, 164, 17–25.
Wirth, E.A., and Long, M.D. (2014) A contrast in anisotropy across mid-lithospheric discontinuities beneath the central United States—A relic of craton formation. Geology, 42, 851–854.
Xu, Y., Shankland, T.J., and Duba, A.G. (2000) Pressure effect on electrical conductivity of mantle olivine. Physics of the Earth and Planetary Interiors, 118, 149–161.
Yang, X., Keppler, H., McCammon, C., Ni, H., Xia, Q., and Fan, Q. (2011) Effect of water on the electrical conductivity of lower crustal clinopyroxene. Journal of Geophysical Research, 116, B04208.
Yang, X., Keppler, H., McCammon, C., and Ni, H. (2012) Electrical conductivity of orthopyroxene and plagioclase in the lower crust. Contributions to Mineralogy and Petrology, 163, 33–48.
Yang, B., Egbert, G.D., Kelbert, A., and Meqbel, N.M. (2015) Three-dimensional electrical resistivity of the north-central USA from EarthScope long period magnetotelluric data. Earth and Planetary Science Letters, 422, 87–93.
Yoshino, T., Matsuzaki, T., Yamashita, S., and Katsura, T. (2006) Hydrous olivine unable to account for conductivity anomaly at the top of the asthenosphere. Nature, 443, 973–976.
Yoshino, T., Matsuzaki, T., Shatskiy, A., and Katsura, T. (2009) The effect of water on the electrical conductivity of olivine aggregates and its implications for the electrical structure of the upper mantle. Earth and Planetary Science Letters, 288, 291–300.
Yuan, H., and Romanowicz, B. (2010) Lithospheric layering in the North American craton. Nature, 466, 1063–1068.

Manuscript received December 24, 2020
Manuscript accepted March 12, 2021
Manuscript handled by Zhicheng Jing

Endnote:

[1]Deposit item AM-22-37942, Online Materials. Deposit items are free to all readers and found on the MSA website, via the specific issue's Table of Contents (go to http://www.minsocam.org/MSA/AmMin/TOC/2022/Mar2022_data/Mar2022_data.html).